RESEARCH ARTICLE

A Simple, Inexpensive System for Digital Particle Image Velocimetry (DPIV) in Biomechanics

WILLIAM G. RYERSON* AND KURT SCHWENK
Department of Ecology and Evolutionary Biology, University of Connecticut, Connecticut

JOURNAL OF EXPERIMENTAL ZOOLOGY
PART A
ECOLOGICAL GENETICS AND PHYSIOLOGY
A Journal of Integrative Biology

ABSTRACT

Functional morphology and biomechanics seek to reveal the mechanistic bases of organismal functions and the physical principles involved at the phenotype–environment interface. Characterization of fluid flow (air or water) within and around organismal structures is an example of this approach. Digital particle imaging velocimetry (DPIV) has been exploited in a variety of biological systems to visualize fluid flow associated with animal movement. DPIV employs particles suspended in air or water that are illuminated by a laser light sheet and recorded with a high-speed video camera. Software tracks particle movement across a specified number of video frames, generating vector diagrams showing patterns of fluid flow through time. As powerful as DPIV methods are, they are limited in application by the high cost and complexity of the equipment required. In this article, we describe a simple DPIV system that substitutes widely available, inexpensive consumer components for scientific-grade equipment to achieve low cost (<$1,000 total) and high accuracy (total error calculated to be approx. 6%, as compared with 5% in professional systems). We have employed this system successfully in our studies on the fluid dynamics of chemosensory tongue-flicking in snakes. This system can be used for research and teaching in labs that typically cannot afford the expense or commitment of a traditional DPIV apparatus and is particularly suited for obtaining preliminary data required to justify further grant and institutional support. *J. Exp. Zool. 313A, 2011.* © 2011 Wiley Periodicals, Inc.

J. Exp. Zool. 313A, 2011

How to cite this article: Ryerson WG, Schwenk K. 2011. A simple, inexpensive system for digital particle image velocimetry (dpiv) in biomechanics. J. Exp. Zool. 313A:[page range].

The fields of functional morphology and biomechanics traditionally seek to explain how organisms are structured and how they use their parts to accomplish the mechanical tasks necessary for living. Structures of interest can be associated with any aspect of an organism's biology. Although the value of understanding the function of a structure and its performance is undeniable, for many questions in biomechanics, these alone do not provide a complete picture, particularly in an evolutionary context. As such, biomechanics research over the last 25 years has increasingly focused on the physical interaction between an organism and its environment. How an individual interacts with the environment, both in terms of moving within it, and acquiring resources from it, can have a vast impact on that individual's life history and relative fitness. Thus, detailed analyses of biomechanics can not only show how organisms "work" in a mechanistic sense but also reveal individual differences at the organism–environment interface that underlie variation in organismal performance, and therefore fitness (Arnold, '83; Koehl, '96). Thus, biomechanics can play a large role in our understanding of phenotypic evolution (e.g., Herrel et al., 2008; Bergmann and Irschick, 2010).

A variety of experimental techniques have been developed to examine the physical interface between an organism and its environment in relation to movement. Digital particle image velocimetry (DPIV) is a method that allows visualization of fluid (air or water) movement under experimental conditions. Of particular interest in biological studies is visualization of the fluid

Grant Sponsor: Wetzel Fund of the Department of Ecology and Evolutionary Biology; University of Connecticut Research Foundation.

*Correspondence to: William Ryerson, Department of Ecology and Evolutionary Biology, University of Connecticut, 75 North Eagleville Road, Storrs, CT 06269-3043. E-mail: william.ryerson@uconn.edu

Received 10 April 2011; Revised 24 August 2011; Accepted 10 October 2011

Published online in Wiley Online Library (wileyonlinelibrary.com). DOI: 10.1002/jez.725

as it comes into contact with an object or surface (Raffel et al., 2000; Adrian, 2005; Lauder and Madden, 2008). This might involve a stationary object with fluid moving past it, or an object moving through the fluid. To accomplish this, the fluid is seeded with neutrally buoyant particles that remain suspended within it. These particles are illuminated with a laser light source that is passed through one or more collimating lenses until a flat plane or sheet of light is produced. Any particles positioned in this plane reflect the laser light and can be recorded using a high-speed video camera. As such, particles set into motion by movement of the fluid around an object or by movement of the object, itself, are illuminated within the laser light sheet and incremental changes in particle position through time are recorded in sequential video images. Software analysis is then used to track particle movements between image pairs, resulting in a detailed record of particle/fluid movement through time during the behavior of interest. Typically, the software represents averaged particle movements during a specified period of time (i.e., a specified series of video frame pairs) as vector diagrams illustrating both particle direction and velocity. Vector isoclines are often used to generate false-color images that illustrate patterns of fluid velocity (in $msec^{-1}$) and direction, as well as second level parameters such as vorticity (fluid rotation, in units of sec^{-1}).

DPIV has been used extensively to examine both feeding and locomotion in aquatic animals, particularly fishes (e.g., Day et al., 2005, 2007; Holzman et al., 2008; Lauder and Madden, 2008; Nauwelaerts et al., 2008; Lauder, 2011). Microscopic, coated glass spheres act as seeding particles, remaining neutrally buoyant in the water column. Often, water flumes are used with suspended beads while swimming organisms match the velocity of the flow, holding station in one position, allowing videography of a "moving" animal or an object fixed in the stream.

DPIV studies of terrestrial (including flying) organisms can be more challenging owing to motility of the animals and the difficulty of creating particles that remain suspended in air for long enough to permit recording. Often a wind tunnel is substituted for a water flume so that flying animals can be recorded while remaining in more-or-less the same position. The majority of recent DPIV applications to terrestrial systems have focused primarily on the patterns of air movement generated during animal flight in a variety of taxa, from moths to birds (e.g., Tobalske, 2007; Mountcastle and Daniel, 2009; Altshuler et al., 2009; Hedenström et al., 2009; Spedding and Hedenström, 2009; Tobalske et al., 2009).

Despite the power of DPIV and the broad utility of this technique within biomechanics, its availability has been severely limited owing primarily to the high initial cost of the necessary equipment. The typical DPIV system employs several specialized components, including a laser light source (typically a class 4, neodymium:YAG or neodymium:YLF laser), a set of lenses to collimate the light beam into a flat sheet, and a high-speed video camera. For seeding particles in the air, a Laskin nozzle aerosol generator is often used to produce fine particles of olive oil, approximately 1 μm in diameter, that remain suspended in the air for hours at a time. For aquatic systems, minute, neutrally buoyant glass spheres are used as seeding particles. Finally, professional DPIV systems usually include proprietary software that is required to analyze particle movement in the video sequences. Even with recent, significant reductions in the cost of some components (notably high-speed cameras), a complete DPIV system can still cost tens of thousands of dollars. Research-grade, high-speed video cameras capable of shooting up to 1,000 frames per second (fps) or faster, alone, presently cost between $5,000 and $100,000+.

The purpose of this article is to describe a simple, inexpensive DPIV system that we have used successfully in our studies of animal biomechanics, specifically tongue-flicking in snakes in both air and water (Ryerson and Schwenk, in preparation). The system is flexible enough to be adapted to use with other organisms and behaviors. By substituting relatively inexpensive consumer products that have recently become available for much more expensive, commercial grade research equipment, taking advantage of open-source analytical software that is now available online and combining these with novel techniques and materials, we have compiled a simple-to-use DPIV system for less than $1,000. We hope that the low cost and ease of use of this system will encourage a much broader application of DPIV methods in research and teaching.

THE EXPERIMENTAL APPARATUS FOR DPIV IN AIR

Our DPIV system consists of the same basic components described earlier for specialized systems, with a few modifications (Table 1, Fig. 1). As a laser light source, we used a high-power laser pointer with attached lenses to modify the light beam into a light sheet. Specifically, we used a NOVAlaser X75® (NOVAlasers Inc., Toronto, Canada) laser pointer operating with a power output of 75 mW at 532 nm (a class IIIb laser). The laser is powered by two AAA alkaline batteries. A NOVAlaser collimating lens was attached to the laser pointer to create a light sheet of 2 mm thick. This was placed in a clamp and directed toward the side of a 20-gallon long aquarium. A mirror was placed on the opposite side of the aquarium, perpendicular to the laser sheet, to reflect the remaining laser light directly back at the source, enhancing the amount of illumination. Laser pointers of varying strengths have been used previously in other studies, and have been shown to provide adequate power to illuminate seeding particles (Mountcastle and Daniel, 2009). Since the laser pointer is not as bright as more powerful lasers, we conducted our experiments in a darkened room. This helps to increase the contrast between the background and the reflected light from suspended particles, aiding in video analysis (see below). Another way to improve contrast would be to use a bandpass filter that emphasizes light frequencies in the range of the laser light source (in this case, a 532-nm bandpass filter). In our experiments thus

Table 1. Equipment and software used in our low-cost DPIV system with contact information and approximate costs.

EQUIPMENT	LINK	QUANT	APPROX COST (USD)
Cameras			
Casio EX-FH100® digital camera	casio-intl.com/dc/	1	$250
OR			
Fujifilm FinePix® HS10 digital camera	fujifilm.com/products/digital_cameras	1	$370
16 GB SDHC memory card		1	$20
Laser			
NOVAlasers X75 Compact Portable >75mW Laser®	novalasers.com	1	$170
NOVAlasers X-Series Lens Holder with Optics®	novalasers.com	1	$23
Software			
MATLAB®—student version, academic license	mathworks.com/products/matlab		$100
PIVlab®—Time-Resolved DPIV Tool for Matlab	pivlab.blogspot.com		Freeware
Avidemux®	fixounet.free.fr/avidemux/		Freeware
AhaView®	aha-soft.com/ahaview		Freeware
Miscellaneous			
Personal computer (PC) (adaptable to Mac)		1	–
Aquarium (20 gal. long)		1	$60
Tripod (to support camera)		1	$50
Cornstarch		1	$2
Chlorococcum aquaticum culture	www.utex.org	1	$30
Compressed air		1	$9
AAA batteries (for laser)		2	$5
AA batteries/rechargeable (for camera)		4	$20
Laboratory clamp to hold laser		1	–
Mirror		1	–
		TOTAL COST:	$739–$859

Note that specific models of consumer equipment and their costs change frequently and vary across countries, but models with comparable functions and comparable or lower cost usually remain available.

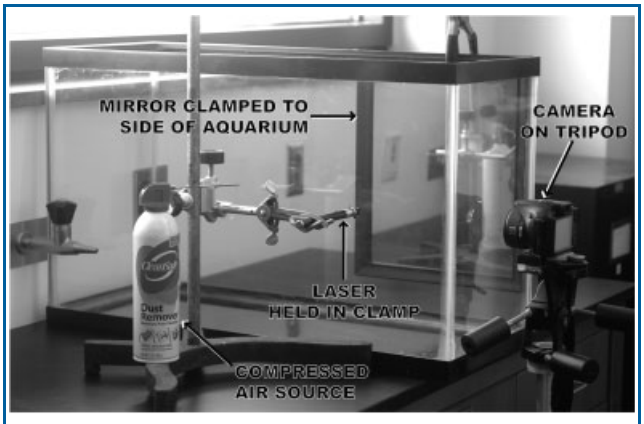

Figure 1. Photograph illustrating the simple apparatus used for DPIV of animal movement in air and water. DPIV, digital particle imaging velocimetry.

far we have not used bandpass filter, but it is possible to purchase a relatively broad spectrum one (375–635 nm) at low cost (approx. $75).

Rather than a Laskin nozzle aerosol generator and olive oil for seeding the air with reflective particles, we used household, processed cornstarch, available in any supermarket (Wang et al., 2006). A small pile of cornstarch was placed on the bottom of the aquarium below the camera's field of view. Before filming, a short burst of compressed air (canned or from a hose connected to a lab bench nozzle) was directed at the cornstarch, causing a cloud of cornstarch to rise from the bottom. After approximately 15 sec, the heaviest dust particles settle to the bottom, whereas the smallest particles remain suspended in the air for another 45 sec to a minute. Seeding density is remarkably uniform across the field (Fig. 2A). The cornstarch particles are spheroidal and relatively uniform in size (approx. 10–18 μm), with most particles about 15 μm in diameter (Fig. 3; Yang et al., 2005). The cornstarch particles have a relatively low density (approx. 1,550 kg/m^3) and the smallest particles weigh very little (approx. 1.22×10^{-10} g); hence their ability to remain suspended for a minute or more (settling velocity is discussed further below in the discussion of error estimation). They are highly reflective and clearly visible while illuminated within the laser light sheet

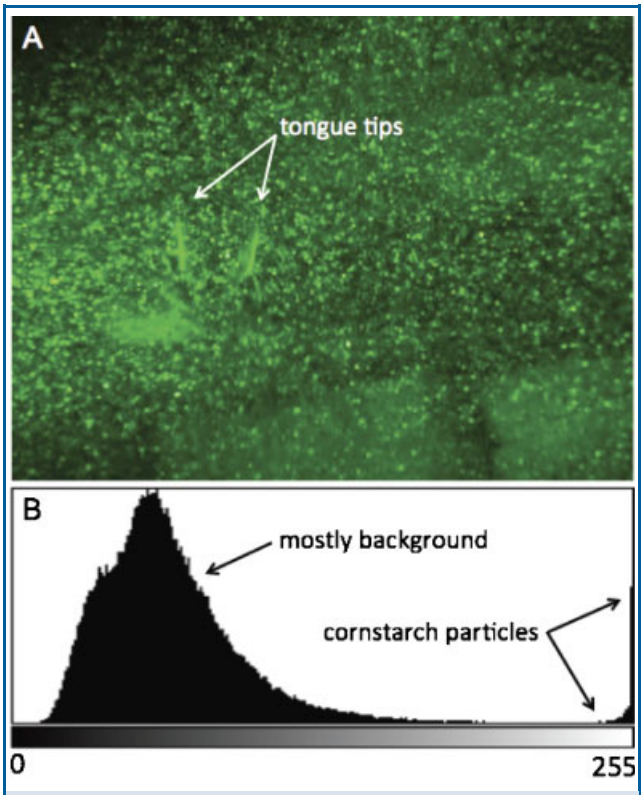

Figure 2. (A) Single high-speed video frame showing suspended cornstarch particles illuminated in laser light sheet. The tips of a snake's forked tongue are indicated as they sweep through the light sheet, moving the air and the particles (Fig. 4). From Ryerson and Schwenk (in preparation). (B) Histogram showing the 16-bit grayscale distribution (255 levels) for the video frame shown in (A) *before* image preprocessing by the software to enhance contrast. The histogram reveals two peaks, with the dark background represented in the large peak on the left and the bright, reflective cornstarch particles indicated by the narrow peak along the right-hand margin. This pattern indicates the excellent contrast provided by the suspended cornstarch particles in the laser light, which facilitates software analysis of particle movement (see text).

(Fig. 2A). Any movement of the air disturbs the particles and any particles moving within the 2-mm thickness of the laser light sheet can be recorded with a high-speed video camera placed perpendicular to the plane of the sheet.

To capture particle movement, we used a Casio EX-FH25® consumer grade digital camera (10.1 MP High-speed Digital Camera with 20× Wide Angle Zoom, CMOS Shift Image Stabilization and 3.0 inch LCD; Casio Computer Co., Tokyo, Japan) with a 16-GB SDHC memory card (Table 1). The camera has settings for 30, 40, 120, 240, 420, and 1,000 fps. Normal speed movies at 30 fps can be shot in "high definition"

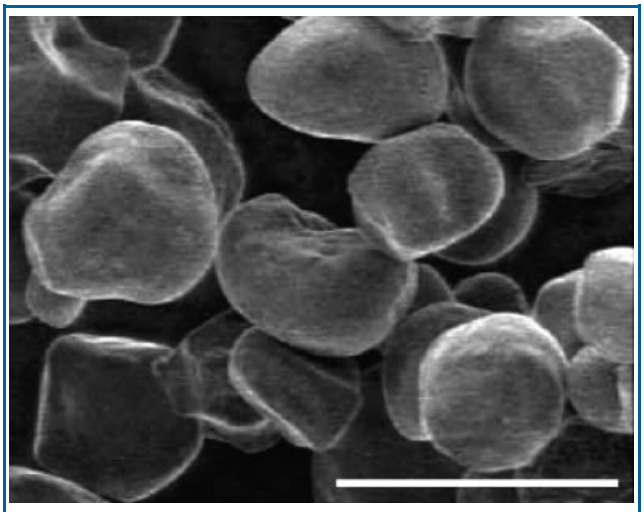

Figure 3. SEM image of cornstarch particles illustrating spheroidal shape and an average diameter of 15 μm (modified from Yang et al., 2005). Scale bar = 20 μm.

(1,280 × 720 pixels) and in addition, a single burst of 40 frames at 40 fps can be shot at full camera resolution (3,648 × 2,736 pixels) using a buffering system and trigger that allows one to capture a rapid movement after it has happened. At 120, 240, 420, and 1,000 fps, camera resolution is 640 × 480, 448 × 336, 224 × 168 and 224 × 64 pixels, respectively. Shutter speed is adjustable and can be as short as 1/5,000th of a sec. At the time of this writing, however, the Casio EX-FH25 has been discontinued. It has been replaced by the Casio EX-FH100® with more-or-less comparable features. Another camera that would work just as well for this application, but which we have not tried ourselves, is the Fujifilm FinePix HS10® digital camera (10 MP CMOS Digital Camera with 30× Wide Angle Optical Zoom and 3-Inch LCD; Fujifilm Corp., Tokyo, Japan) (Table 1). Both Casio and Fujifilm also make more expensive camera models with additional features and somewhat higher resolution when filming at high-speed: the Casio EX-F1® (approx. $2,900) and the Fujifilm FinePix HS20® (approx. $500). For kinematic studies of snake tongue-flicking (see below), we typically use 420 fps, but for the DPIV analyses, we found that 240 fps is sufficient to capture the comparatively slow fluid movement and that the additional resolution (448 × 336 pixels) is necessary for particle motion analysis, particularly since we are usually interested in analyzing only a portion of the full frame (typically 223 × 258 pixels; see discussion of error estimation, below).

A 2-min video sequence shot at 240 fps has a file size of 660 MB. As such, a 16-GB memory card can hold approximately 24 such sequences (or 48 min of video), providing ample storage. Memory cards are easily changed if additional memory is required. Obviously, longer video sequences or sequences taken

at a higher frame rate will produce files of larger size that fill the memory card faster.

MODIFICATIONS FOR DPIV IN WATER

As noted in the introduction, DPIV is often applied to aquatic organisms using water seeded with neutrally buoyant glass spheres. One part of our studies of tongue-flicking in snakes involves comparing tongue kinematics and fluid dynamics in air to those of the same snake tongue-flicking in water (e.g., in water snakes, *Nerodia sipedon*). Commercially available glass seeding particles are very costly. We therefore sought an inexpensive substitute. We found that cultured green algal cells (specifically *Chlorococcum aquaticum*) worked very well (Table 3). These single-celled, freshwater algae are approximately spherical in shape and only slightly denser than the surrounding water (Oliver et al., '81); hence, their sinking velocity is negligible over the time periods of our application (the median sinking rate of cells in still water is 0.5 cm in 12 min)—for all intents and purposes, the cells are neutrally buoyant. It is worth noting that cells in younger cultures have lower densities and slower sinking velocities than in older cultures (Oliver et al., '81), so we used only young cultures in our studies. Cells are approximately 12 μm in diameter (they range from about 9 to 19 μm; Oliver et al., '81); hence, they are nearly the same size as the cornstarch particles, which for purposes of analysis and error estimation, gives them many of the same advantages (see below). A signal benefit of using algae in our system is that they are green and thus have exceptionally high reflectance in the green laser light. This provides good contrast against the background and facilitates software analysis of particle movement (see discussion of error estimation, below).

Cultures of *Chlorococcum aquaticum* are available from the algae culture facility at the University of Texas, Austin, for a modest price to academic institutions (http://www.utex.org). The culture was grown in our lab using a growth medium (Bristol medium) modified from Bold ('49); the original recipe is provided online at the facility's website and we provide a modified recipe in Table 3. The stock culture was diluted 10 times, then grown in large flasks on a lab bench exposed to sunlight. Growth was rapid and within 2 weeks we had large populations dense enough for seeding our 20 gal. aquarium. The aquarium was filled two thirds with water and a flask of algae drawn from the growth containers was poured in. The appropriate quantity of algae-seeded water added to the aquarium was empirically determined (it depends on the density of one's population)—we strove for a cell/particle density within the aquarium that approximated (by eye and after initial video trials) that of the suspended cornstarch particles (Fig. 2A) because we had found that this density provided good resolution of fluid movement for the video analysis.

Table 2. Error estimation in DPIV analysis of cornstarch particle movement in air using the methods proposed here.

Variable	Error estimate
Particle-fluid infidelity	2.32%
Bias error	1.40% ± 0.03%
Optical distortion	1.00%
Correlation peak	0.80%
Peak locking	0.50%
Total estimated error	6.02% ± 0.03%

Total error is only slightly greater than the ~5% error reported for high cost commercial systems (see text). Total error for algal particle movement in water is significantly less than the 6% calculated for cornstarch in air and is therefore within the range of commercial systems (see text). DPIV, digital particle imaging velocimetry.

VIDEO MOTION ANALYSIS

As noted, costly, high-end professional DPIV systems often include proprietary software to analyze particle movement, but recently, very powerful, no cost, open-source software has become available that performs most of the same tasks. The program we used is PIVlab® (http://pivlab.blogspot.com/), developed by William Thielicke and Eize J. Stamhuis (Table 1). Although PIVlab is available for free, it is designed as a module or tool to run on the commercially available computational platform, MATLAB® (MathWorks, Natick, MA), which must be purchased (Table 1). We ran all software on a PC using a Windows® operating system.

PIVlab analyzes video image pairs and measures the direction and distance of particle displacement. By compiling a series of image pairs in a specified video sequence, the software calculates average particle velocity and direction within the specified time period. It can also calculate secondary parameters such as "vorticity"—the degree of fluid circulation within a given area (Vogel, '94, 2003). The software is also able to correct for the gravitational settling of the relatively heavy cornstarch particles during video recording, subtracting this component of particle motion from its calculations (see below). Output consists of a grid of vectors indicating particle movement emphasized by false-color backgrounds representing isoclines of fluid velocity or vorticity (Fig. 4). The software had no trouble in analyzing movement of the laser-illuminated cornstarch particles and algal cells we used in our experiments. The specific parameters we used in analyzing particle movement are given in the discussion of error estimation, below.

For analysis, high-speed videos need to be separated into individual sequences of focal behaviors (in our case, individual tongue-flick clusters). We used open-source video editing software, Avidemux® (developed by Mean, fixounet@free.fr, released under the GNU General Public License [GPL]), but a variety of video editing programs are available to do this. For PIVlab analysis, video frames need to be converted into 16-bit grayscale JPEG images. We used another open source program,

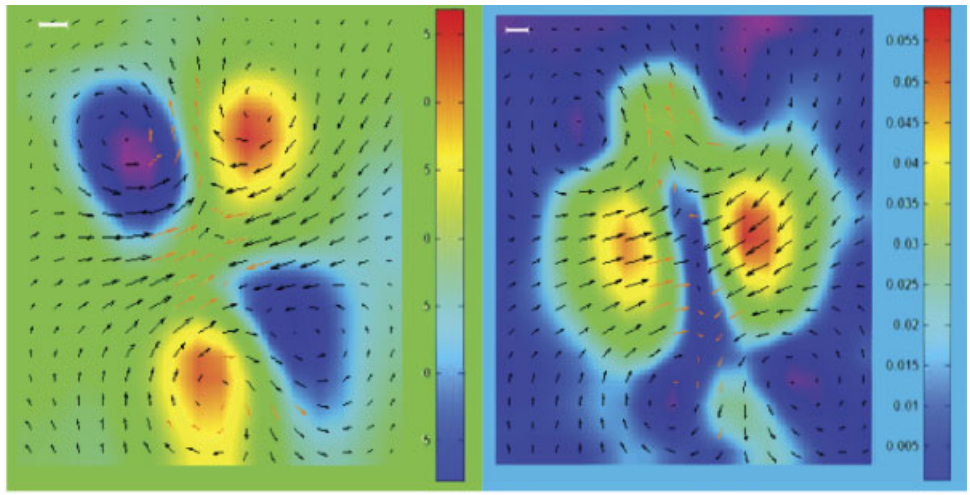

Figure 4. Examples of PIVlab software analysis output revealing patterns of particle (i.e., air) movement generated by a snake's (*Thamnophis sirtalis*) tongue during chemosensory tongue-flicking. Each figure represents analysis of the same pair of video frames such that one image could be superimposed on the other. At this point in the kinematic sequence, the tongue tips are above the image frame and behind the laser light sheet. The images show a portion of the full video frame, i.e., an "area of interest," designated by the user—in this case, 223 × 258 pixels. In both figures, the direction and magnitude of air movement are represented by vectors. Orange vectors represent values interpolated by the software owing to spurious or missing data points, usually because tracked particles have left the plane of the laser light sheet between video frames. Isoclines of magnitude (either "vorticity" or velocity) are shown by patterns of false color, with quantitative values indicated by the color scale to the right of each image. Data were smoothed using a single 3 × 3 pixel pass applied by the SMOOTHN algorithm within the PIVLab softward (based on Garcia, 2010). (**A**) Air vorticity, or circulation (in abstract units of "per secs," sec^{-1}). Vorticity is caused by shear between stream lines in turbulent flow within a fluid resulting in translational movement that is technically distinct from rotation (see Vogel, 1994, 2003). Clockwise circulation is indicated by warm colors and counterclockwise circulation by cool colors. Note that the angular velocity of fluid is highest in the center of each vortex, which is typical of irrotational flow. The upper pair of counter-rotating vortices is generated by the tongue tips as they move upward during a flick cycle; the lower pair is generated by the downward-sweeping tongue tips. Each sequential flick in a oscillatory, multiflick bout reinforces the vortices. During a downward sweep the tongue tips move through the inner margins of the upper vortices and then through the inner margins of the lower vortices during the upward sweep, creating a counter-current flow pattern between the tongue tips and the surrounding air during both the down stroke and the upstroke of a flick cycle. We believe that the vortices function as part of a mechanism serving to increase the rate of odor molecule collection on the tongue tips by increasing the encounter rate of the tongue tips with odor molecules, as well as the rate of diffusion of these molecules into the sero-mucous fluid covering the tongue tips (Schwenk, 1996; Filoramo and Schwenk, 2009; Schwenk and Ryerson, in preparation; Ryerson and Schwenk, in preparation). Scale bar for vectors = 0.05 m sec^{-1}. (**B**) Air velocity ($msec^{-1}$). Warmer color indicates higher velocities as shown by the color scale. This figure demonstrates that the highest air flow velocities (approx. 0.06 m sec^{-1}) occur in the intermediate zone between upper and lower pairs of vortices. As the tongue tips sweep up-and-down, the vortices draw fresh air in from the sides and eject it vertically. This pattern of air movement represents an effective mechanism of convection to replace the supply of odor molecules that might become depleted in the boundary area near the tongue tips (see citations above). Scale bar for vectors = 0.05 m sec^{-1}.

AhaView® image editing software (Aha-Soft, Vancouver, Canada) to do the conversion (Table 1).

ESTIMATING ERROR IN THE SYSTEM

Error Estimation for Cornstarch Particles in Air

When developing a new methodology, or modifying an established one, it is important to assess accurately the potential error in the quantitative results. Error estimation in PIV has been dealt with in the technical, engineering literature (e.g., Raffel et al., 2000 and other references cited below) and for a biological application by Tobalske et al. (2009). There are two major sources of inaccuracy in PIV studies—systematic and residual (Raffel et al., 2000). Systematic errors stem from the cross-correlation algorithm being applied to the image pairs. Residual errors are the result of uncertainty in measurement. Separating the two types of error is often difficult, and it is usually easier to calculate the total error as the sum of a random measurement error and a

bias error (Eq. 1).

$$\varepsilon_{tot} = \varepsilon_{bias} + \varepsilon_{rms} \quad (1)$$

The bias error represents inaccuracies in the estimation of the displacement vector for a sequential image pair, represented as deviation from the mean of surrounding vectors (Fincham and Spedding, '97; Huang et al., '97). The random measurement error is a combination of several factors: particle to pixel size, particle-fluid infidelity (shear), "peak locking", interrogation area size and frequency distribution of light intensity can all contribute to the total error in the analysis (Table 2).

In biological research, the typical total error for commercially produced PIV systems is in the vicinity of 5% (Tobalske et al., 2009). The application of an inexpensive PIV technique, as reported here, would be impractical if the resulting uncertainty were much higher than this benchmark. We calculated the potential error inherent in our methods by breaking the methodology down into its components, examining each component for error and running control experiments, allowing us to calculate the total amount of error that could arise using this technique. A final source of error, optical distortion (error resulting from the curvature of the camera lens) is conservatively estimated at 1% (following Raffel et al., 2000).

Frequency distribution of light intensity. The software's ability to analyze particle images is heavily dependent on the detection of individual particles. The software uses a "threshold" gray value for bright particles on a dark background (in an 16-bit grayscale there are 255 values). Pixels that exceed the threshold value (i.e., are relatively bright or toward the white end of the value scale) are considered particle images, others are deemed background signal. A histogram of pixel gray values can be used to determine where this threshold should be established. The use of a single value for the threshold assumes uniform illumination of the seeding particles. Ideally, this would result in a histogram with a bimodal distribution, one peak for the background signal and one for the particles. In practice this is usually not the case (McKeon et al., 2007). The most common result is a single peak with a long tail. The peak values represent the background signal and the tail values represent particle images. The resulting vectors will then be biased by the set threshold, the size of the particle (larger particles reflect more light), and the position of the particle in the laser sheet (particles in the center reflect more light). These biases can be alleviated (although not eliminated) by preprocessing of the image to optimize the contrast between the background noise and the particle images. Preprocessing techniques include histogram equalization and the use of high-pass filtering. This results in a distribution of gray values that more closely approximates uniform. PIVLab automatically preprocesses images to optimize contrast before calculating particle motion vectors. In our case, raw images (before software pre-processing), in fact, produced grayscale histograms that were bimodal (Fig. 2B), indicating a sharp delineation between background and particle values.

Table 3. Information on *Chlorococcum aquaticum*, the freshwater alga used as seeding particles in our water-based DPIV system (see text).

Chlorococcum aquaticum	
Shape	Approximately spherical
Diameter	9–19 μm
Density	1.02–1.09 gm/cm^3
Sinking velocity	1.5–8.2 × 10^{-4} cm/sec
Growth medium ingredients	
Ingredient	Quantity
dH_2O	1 L
$NaNO_3$	7.2 g
$CaCl_2 \cdot 2H_2O$	0.24 g
$MgSO_4 \cdot 7H_2O$	0.72 g
K_2HPO_4	0.72 g
KH_2PO_4	1.68 g
NaCl	0.24 g
Growth medium directions	
1.	Starting with the $NaNO_3$, mix each of the chemical ingredients, in order, into 1 L of deionized water while stirring continuously
2.	Cover and autoclave the medium solution
3.	Store in a refrigerator until ready to use
4.	Bring to room temperature. Add algal culture sample to growth medium solution.
5.	To 1 part medium/alga solution, add 9 parts of dH_2O
6.	Place each diluted aliquot into a large glass container
7.	Place container in sunlight for population growth (approx. 2 weeks, depending on initial population size and environmental factors)

Data are for *Chlorococcum* spp. and taken from Oliver et al. ('81). The recipe for growth medium is based on Bold ('49; see http://web.biosci.utexas.edu/utex/mediaDetail.aspx?mediaID = 29) and modified by Univ. of Connecticut phycologist, K. Fucikova (personal communication).

Interrogation area size. The area of interrogation is a window within the field of view used by the correlation algorithm to detect the patterns of particle movement. The size of the interrogation window is typically chosen based on the particle density (Raffel et al., 2000). When particle density is low, larger interrogation windows can compensate, but at the cost of reducing fluid flow resolution. At higher particle densities,

smaller interrogation windows enhance the number of vectors resolved by the algorithm but also increase the likelihood of spurious vectors occurring in the analysis. Most modern software and algorithms rely on a multipass approach, starting at an interrogation window of 64×64 pixels, and after multiple iterations, concluding at 16×16 pixels with a 50% overlap (Tobalske et al., 2009). Here we use a similar multipass approach for analysis. Our final output shows particle/fluid movement over an area of interest of 223×258 pixels (Fig. 4).

''Peak locking,'' Correlation Peak, and Particle Sinking. The novel use of cornstarch particles as a seeding material in our method requires some additional consideration. In typical commercial systems, the use of aerosolized olive oil results in particles $<1\,\mu m$ in diameter, which is small compared with pixel size in the video. The mean diameter of cornstarch particles is approximately $15\,\mu m$ (Fig. 2; Yang et al., 2005). As such, particles are large enough to span several pixels (in practice, 2.5 pixels). The large particle size relative to pixel size minimizes the bias error associated with overestimating vector displacement, a result of ''peak locking,'' such that the error is less than 1% (Fincham and Spedding, '97; Raffel et al., 2000). Peak locking occurs at small particle to pixel size ratios when estimations of velocity can become ''fixed'' at particular values, typically integers (Fig. 5.25 in Raffel et al., 2000). Our large particle size to pixel size ratio minimizes the potential effects of peak (or integer) locking, resulting in an even distribution of particle displacement (velocity) values (Fig. 5). We therefore estimate this error at 0.5%.

At a particle size of $15\,\mu m$/2.5 pixels, a Gaussian peak fit estimator (Raffel et al., 2000) provides the best estimation of a correlation peak at 0.1 pixels. The maximum particle displacement measured in our experiments was approximately 8 pixels, which approximates a root-mean-square error of 0.8% (Deng et al., 2004).

The disadvantage of larger particles is their greater mass so that analyses must account for their (vertical) settling velocity owing to gravity. PIVLab allows the user to measure this settling velocity directly and remove this component of particle movement from the analysis automatically. As such, the average vertical velocity is calculated from the entirety of the region of interest and this reference vector is subtracted from total particle movement. To check the accuracy of the software, we calculated cornstarch particle settling velocity by hand using serial images from a high speed video sequence (Eq. 2; Prasad, 2000):

$$u_\infty = g d_\rho^2 (\rho_\rho - \rho_f)/18\mu \qquad (2)$$

where u_∞ is the settling velocity, g is acceleration due to gravity, d_ρ is the diameter of the particle, ρ_ρ and ρ_f are the densities of the particle and fluid, respectively, and μ is the viscosity of the fluid. The average settling velocity for cornstarch, as reported by the PIVlab software, was 0.07 cm/sec; calculated by hand it was found to be 0.063 cm/sec. This small error is included within the total ''bias error'' measured experimentally and discussed below.

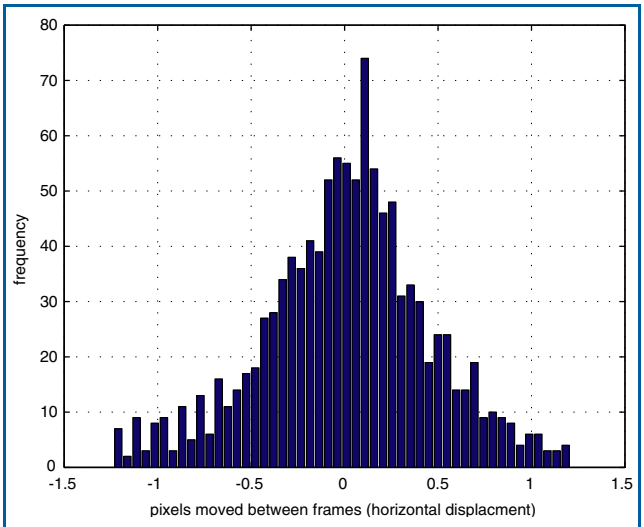

Figure 5. Histogram showing the frequency distribution of (horizontal) pixel displacement of cornstarch particles between two sequential video frames at 240 fps (i.e., number of pixels moved in 4 ms). A single peak in the distribution around 0 indicates that particle size relative to pixel size in our video is sufficient to avoid ''peak locking'' error (also known as ''integer locking'') in the analysis, which can occur if particles are too small relative to the resolution of the video image (see text). If peak locking had occurred, the distribution of the histogram would have been trimodal, with peaks at -1, 0, and $+1$ (see text and Fig. 5.25 in Raffel et al., 2000).

Particle-Fluid Infidelity. Another potential drawback of using larger, heavier (cornstarch) particles is their greater inertia. Ideally, a PIV seeding material would move with the surrounding fluid instantly, with perfect fidelity and no lag. In practice, almost any particle will have an inertial component that introduces error in calculating flow direction and velocity. This particle-fluid infidelity (shearing or "slip velocity"; see below) can have a discernable impact on the analysis depending on its degree. In calculating this error, we assume that the effects of added mass, unsteady drag forces, and nonuniform fluid motion are negligible (Adrian, 2005) and instead focus on diameter and density of the particle, as well as the slip velocity (Deng et al., 2004). The slip velocity is defined as the difference in the velocity magnitude between the movement of the fluid and the seeding particles. Using a known air flow and comparing this with the measured particle velocities can therefore provide an accurate assessment of the slip velocity.

To examine the slip velocity of cornstarch, a jet of compressed air (CleanSafe Dust Remover®, IQ Products, Houston, TX) was shot in line with the laser sheet while being videotaped at 240 fps.

The distance that cornstarch particles directly in front of the jet were carried in 10 video frames was used to calculate particle acceleration. The velocity of the airstream was calculated from the application of the continuity equation (Eq. 3):

$$v = Q/\pi r^2 \quad (3)$$

where v is the flow velocity, Q is the flow rate, and r is the radius of the nozzle. The flow rate (Q) was calculated as the loss of volume of air by the can after 3 sec of operation, measured by taking the mass before and after spraying, then converting to volume lost (density of air at 20°C is 1.2041 kg/m^3). The resulting flow rate was 1.626 cm^3/sec. The radius (r) of the nozzle was 0.5 mm. Therefore, the air flow velocity (v) was determined to be 2.070 cm/sec. Measurement of particle movement at the tip of nozzle resulted in a particle velocity of 2.022 cm/sec; therefore, the difference between air velocity and particle velocity is the slip velocity, which equals 0.048 cm/sec or 2.32% of the air flow velocity (Table 2).

Bias Error. To ascertain the level of bias error in the PIVlab algorithm, a cordless drill was placed in the experimental chamber. The drill was fitted with a small disc with a white dot painted on it 1.4 cm from the center. While being videotaped at 240 fps, the drill was turned on and given time to reach its maximum rotational velocity. The rotational velocity was then calculated both by hand (using the known frame rate of the camera) and using the PIVLab software across a series of speeds. Deviation of the PIVLab measurements from the hand-checked values represents bias error measurement in this test (Fig. 6). When the residuals of software values around the measured line are plotted (Fig. 6B), the slope of the line is not significantly different from zero, so that the y-intercept (0.014) represents a measure of the bias error (i.e., $1.4 \pm 0.03\%$ error; Table 2) (Spedding et al., 2003). The zero slope also shows that the error relative to the actual rotation rate is random, i.e., there is no nonlinearity built into the error of the system.

Total Error Estimate. Using Equation (1), we can combine all the sources of error together, giving us an estimated error for velocity measurement using our system of 6.2% (Table 2). Although this value is slightly higher than the 5% error calculated for professional systems, it remains a reasonable value for scientific application, particularly given the extremely low cost of the system.

Error Estimation for Algae in Water

In terms of accuracy, using algae for DPIV in water has several advantages over cornstarch particles in air. First, algal cells are very similar in size to the cornstarch particles (Oliver et al., '81) and as such, are relatively large compared with pixel size in our videos, thereby minimizing potential peak locking and correlation peak error, as described above. Second, the algae are nearly the same density as the water and are virtually neutrally buoyant. Since they sink very slowly relative to the duration of a typical video sequence, any gravitational component of the bias error is negligible. Second, the algal cells are green and in the green laser light used in this method they provide exceptionally high reflectance and strong contrast with the background, making visualization (and therefore, measurement) more accurate. Given these factors, we have not calculated a specific error estimate for the algal water method described here. It is sufficient to note that measurement error is no greater than—and is very likely less than—the error calculated for cornstarch particles suspended in air. This puts an error estimate close to, if not within, the 5% reported for professional systems (Tobalske et al., 2009).

EXPERIMENTAL EXAMPLE

The DPIV apparatus described here was used in preliminary experiments examining the fluid dynamics of tongue-flicking in snakes, both in air and water (only results for air-flicking are noted here). These data are being prepared for publication elsewhere (Ryerson and Schwenk, in preparation). Here we describe some of our results in order to demonstrate the utility of the system.

Snakes and lizards (squamate reptiles) tongue-flick in order to collect environmental chemicals (odorants) on the tongue tips for olfaction via the vomeronasal organs (Halpern, '92; Schwenk, '95). With very few exceptions, lizards use single tongue-flicks that are directed at the substrate or at a surface; tongue-flicks are only occasionally directed into the air alone (Gove, '79; personal observation). In contrast, snakes routinely tongue-flick in the air without substrate contact (although they often touch the substrate, as well). Furthermore, snakes typically employ bouts of multiple tongue-flicks in which the tongue is rapidly oscillated up-and-down. In order for the tongue tips to serve as chemical collectors in the air, odor molecules must move into the mucous fluid layer coating the tongue surfaces. Therefore, the mechanism of odorant collection is one of diffusion and/or sorption (Schwenk, '96; Filoramo and Schwenk, 2009), just as it is within the mucous layer covering the olfactory epithelium in the typical tetrapod nose (e.g., Schoenfeld and Cleland, 2005). However, these processes are typically very slow and this problem is exacerbated by boundary layer effects (Vogel, '94, 2003). Our hypothesis is that oscillatory tongue-flicking behavior is an adaptation to increase both the encounter rate of the tongue with odorants, as well as the rate of diffusion/sorption of these molecules into the lingual fluid by increasing the steepness of the velocity gradient of airflow at the tongue–air interface, thereby decreasing the thickness of the boundary layer (Schwenk '96; Schwenk and Ryerson, in preparation). It would further promote chemical collection by creating turbulence that would replace depleted odor molecules at the interface. Once odor molecules are collected within the lingual fluid layer, the tongue is retracted into the mouth and the fluid on the tongue tips is transported hydraulically to the vomeronasal fenestrae within the anterior palate where it is then available for secondary transport into the

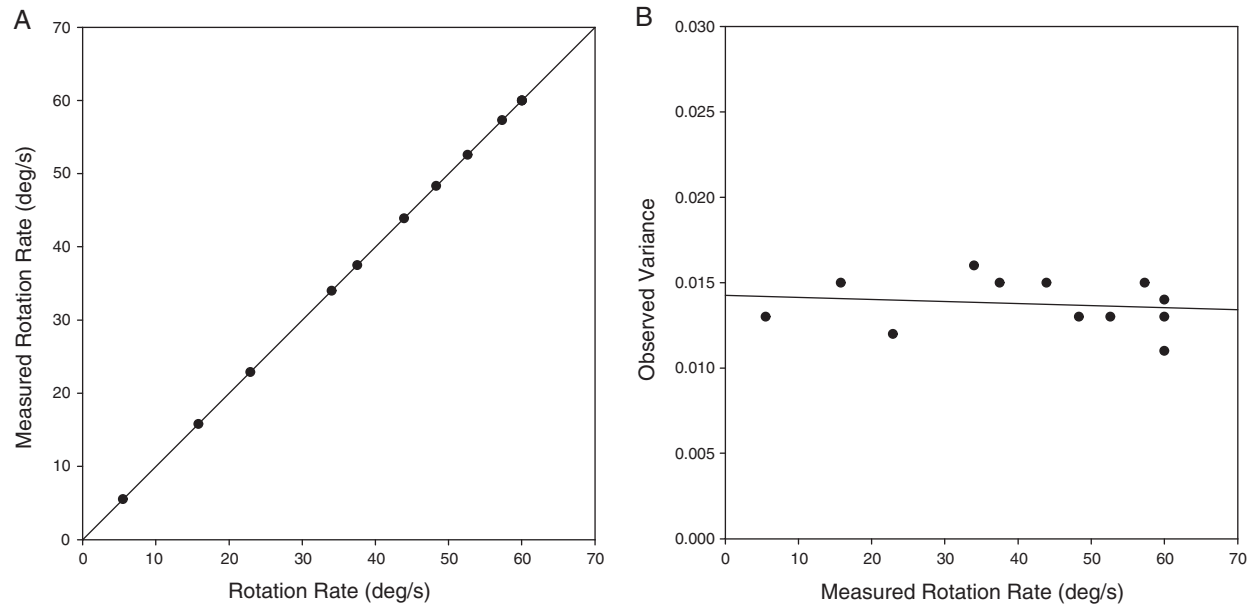

Figure 6. Experimental determination of "bias error" in our DPIV system using directly measured values of angular velocity (rotation rate) vs. software-determined values (see text). The test used an electric drill spinning a small disc with a white dot painted on it to simulate cornstarch particle movement, while videotaped at 240 fps. We analyzed a series of video frames corresponding to the start of the drill so that our measurements would span a large range of rotational speeds. **(A)** In this graph, the solid line represents the angular velocity of the white dot as measured directly from the video sequence of the accelerating drill. The black dots along the line represent the values of angular velocity as determined by the PIVLab software. Although the software values appear to lie directly on the measured line at this scale, there is actually a tiny amount of deviation from the measured rotation rate, as shown in the next figure (note that three data points at 60 deg sec^{-1}—maximum drill rotation speed—are superimposed in this figure and appear as a single point). **(B)** This graph shows the residuals of the values generated by the PIVLab software compared with the actual (measured) rotation rate. A line fit through the residual values is statistically indistinguishable from 0, indicating that there is no consistent trend or nonlinearity in the error and that the *y*-intercept of 0.014 ($1.4 \pm 0.03\%$) accurately represents the system's bias error (Spedding et al., 2003). This small bias error suggests that the PIVLab software performs very well.

vomeronasal lumina for sensory tranduction (Filoramo and Schwenk, 2009; Filoramo and Schwenk, in preparation).

Our preliminary results (Fig. 4) support our hypotheses and provide additional insights. Tongue-flick velocities are, indeed, high (in garter snakes, *Thamnophis sirtalis*, mean down stroke velocity = 0.76 m/sec, mean upstroke velocity = 0.68 m/sec), which would decrease dramatically the thickness of the boundary layer at the tongue tip surfaces. Furthermore, the turbulence generated by the tongue-flicking is organized into two standing pairs of counter-rotating vortices, one pair generated during the down stroke, the other pair during the upstroke (Fig. 4A). We found that it typically takes two to three flick cycles within a bout (mean number of flicks in a bout = 6 ± 0.53) in order to generate the vortices. Mediolateral movements of the tongue tips during each flick are complex—the tongue tips do not pass through simple arcs, but rather move toward and away from one another cyclically as the tongue moves down and up. Presumably, these transverse motions help to generate the vortices, but they also serve to position the tongue tips so that they skim along the inner margins of the upper vortices during the down stroke and the inner margins of the lower vortices during the upstroke. This creates a counter-current flow system on both the down stroke and the upstroke that would further serve to increase the rate of diffusion or sorption of molecules into the lingual fluid. Finally, Figure 4B shows that air velocities are highest (0.6 m/sec) in between upper and lower vortex pairs and that flows here are directed medially and upward at the end of the upstroke (and medially and downward at the end of the down stroke—not shown). As such, a constant supply of fresh air (and odorant molecules) is jetted into the collection zone to replace supplies depleted at the boundary layer, moving through the space in a way the contributes additionally to the counter-current flow pattern.

OTHER POSSIBLE APPLICATIONS OF THE SYSTEM

Traditionally, DPIV research has focused on animal feeding and locomotion. However, there are other possible applications of this method outside of these two research areas, particularly given the low cost and simplicity of the system described here. As suggested by our ongoing studies, the fluid dynamics of chemoreception is one obvious place in which a DPIV approach is likely to be useful. The methods we describe could be applied to other aerial, as well as aquatic systems. Most studies of aquatic chemoreception and odor-tracking in invertebrates, for example, have relied on direct visualization of odor plumes using dyes in a water flume, in combination with mechanical and theoretical models (e.g., Loudon et al., '94; Loudon and Koehl, 2000; Koehl et al., 2001; Crimaldi et al., 2002; Koehl, 2003; Mead et al., 2003; Ram et al., 2008). DPIV visualization of flow around crustracean attenules and aesthetascs, specifically, might provide additional insight into the biomechanics of these odor-tracking systems (e.g., Koehl, 2001; Koehl et al., 2001; Goldman and Patek, 2002; Moore and Crimaldi, 2004). Another chemosensory example might be pheromone release in some insects. Other aspects of small animal behavior might also be amenable to these methods. In addition, plant reproductive systems, particularly mechanisms of seed and pollen dispersal in some species, might benefit from application of DPIV methods, generally and our system, specifically.

ADVANTAGES AND DISADVANTAGES OF THE SYSTEM

Naturally, employing an $800 DPIV system in place of one costing tens of thousands of dollars must come with some trade-offs. Although this is true, depending on the application, these trade-offs might be minimal. The two most significant shortcomings of the system we describe are in the resolution of the high-speed video images and the duration of cornstarch particle suspension. Professional-grade high-speed video cameras are capable of shooting frame rates comparable to those listed here, but at much higher video resolution (typically on the order of $1{,}200 \times 800$ pixels at 500 fps, but in very high end cameras, $2{,}580 \times 1{,}600$ pixels at 800 fps!). The advantage of this is that the camera can resolve much smaller particles and particle movements. In other words, the relevant parameter here is the ratio of particle to pixel size—more (effectively, smaller) pixels mean that smaller seeding particles (e.g., aerosolized olive oil droplets) can be used and these have the error-reducing advantages of greater buoyancy, less mass, and less inertia. Given the relatively low resolution of our system, the relatively large cornstarch particles and algal cells were not only inexpensive alternatives but also necessary to compensate for the larger pixel size. If we had used smaller particles, we would have encountered problems with peak locking described above. Higher resolution also provides a proportionately larger field of view that can be analyzed effectively. Nevertheless, despite the lower resolution of our inexpensive camera, larger particle size compensated for some of the drawbacks and the additional error introduced by inertia was minimal.

Calculation errors resulting from loss of particle identity/individution by the PIVlab software are obvious in the output because they present as occasional, extreme outlier vectors that are disproportionately long. They are easily eliminated from the analysis. In our application, this kind of error occurred once or a few times in each image pair analysis, but was easily corrected. The frequency of this kind of error will depend on the average particle velocities present in one's system. In our case, it would take a particle traveling at $50\,\mathrm{cm\,sec^{-1}}$ to pass through the entire 2 mm thickness of the laser sheet between sequential video frames. However, the maximum particle velocity we observed was only $6\,\mathrm{cm\,sec^{-1}}$, hence only particles very close to the margins of the light sheet and moving away from it were likely to be lost in 4 msec between frames.

Of potentially greater concern is that, despite computational correction for gravitational settling of the cornstarch particles, film time is limited to about 45 sec owing to relatively rapid settling. Olive oil droplets generated by a Laskin nozzle aerosol generator, in contrast, can remain suspended for hours (Raffel et al., 2000; Tobalske et al., 2009). This would be an obvious advantage for animals that will not reliably behave within the short time window afforded by the cornstarch (it is also important in applications for which particle size must be known and uniform). For small air movements, inertial effects of the relatively larger and heavier cornstarch particles might mask fluid movements or introduce an additional source of error. However, our experimental analysis of slip velocity suggested that this error is surprisingly small. Although the addition of a Laskin nozzle aerosol generator would be a large improvement on our system, it would require the concomitant use of a higher resolution camera owing to the peak locking problem introduced when particle size is small relative to pixel size (see above). The addition of these two pieces of equipment, while desirable, would add thousands of dollars, if not tens of thousands, to the cost of the DPIV system.

Although for many organismal functions a maximum frame rate of 1,000 fps is more than sufficient, some biological applications require faster frame rates (10,000 fps or more) unavailable at this time on consumer video cameras. As such, very rapid behaviors requiring faster video sampling rates cannot be accommodated by our system and even at 1,000 fps the resolution becomes problematic. Upgrading to a more expensive Casio EX-F1® camera gains a maximum frame rate of only 1,200 fps, but higher resolution (336×96 pixels at 1,200 fps) compared with the cameras described above. Obviously, minimum resolution and frame rate requirements are dependent on the biological behavior of interest. For example, wing movement in tiny insects is both exceptionally fast and difficult to resolve. Such behaviors require cameras with high speed (10,000+ fps) and the highest resolution possible, not to mention short shutter

speed to eliminate blur in the images. In contrast, a small fish swimming slowly at station in a water flume can be studied using frame rates and resolutions on the order described here.

The inexpensive laser light source we used in our experiments was adequate, but stronger, research grade lasers have the advantage of being much brighter, which in turn makes it possible to shoot videos at much higher frame rates with greater resolution. In low light, the signal-to-noise ratio in a digital image is reduced so that images begin to appear pixilated or are otherwise compromised. High frame rates and/or shorter shutter speeds exacerbate this problem. The brighter the light source, the better the image quality. Higher end cameras are also equipped with better quality light sensors that also help to mitigate this problem. To help with image contrast given our relatively weaker light source, we did our DPIV studies in a darkened room. The snakes were unconcerned about the low light and behaved normally, but some organisms might not be so accommodating.

Another shortcoming of the laser pointer system in this context is its dependence on batteries. The laser draws considerable current and the small batteries cannot maintain a bright enough light for videography longer than about 30 min before they need to be replaced. The problem of frequent battery replacement is mitigated by having at hand several sets of high quality, rechargeable batteries. The camera also uses rechargeable batteries, but has the advantage of an AC power source adapter to eliminate batteries altogether. Conversely, the advantage of battery operation is portability and field application. Another advantage is that high-powered laser pointers such as ours are rated class 3b lasers, as opposed to the class 4 research lasers used in typical DPIV systems. Class 4 lasers are potentially dangerous even when reflected, whereas class 3b lasers are far safer if one is not exposed to the beam directly. Nevertheless, appropriate eye protection is necessary when using either laser type.

One of the signal advantages of the DPIV system we describe here, besides its low cost, is its compact size and portability. Because the electrical components (laser pointer and high-speed video camera) are battery operated, they do not require a source of AC current. Small size, durability, and battery operation mean that the system not only is easily transported from one location to another but can also be employed directly in the field where animals are collected. If a darkened room is not available (e.g., at a field station), a make-shift tent or a commercial, fabric film chamber could be used, instead. The low cost, simplicity, and relative safety of the system also mean that it is appropriate for student use and can be used for educational purposes and student projects in an undergraduate setting. Finally, this system allows for quick, inexpensive pilot studies that can collect sufficient preliminary data to support or discard initial hypotheses and to justify grant or institutional support for more extensive work.

Finally, we note that the system described here could be adapted easily to use with a water flume or wind tunnel. Our interests so far have been in examining flow patterns generated by the complex kinematics of a moving animal part, but for organisms that do not remain stationary, the advantages of moving the fluid past the animal are obvious.

CONCLUDING REMARKS

In naming specific pieces of equipment, software and prices, a methods article such as this will necessarily become dated quickly, particularly given how fast the consumer electronics market changes. We have already noted, above, that the camera we initially used is no longer produced. Nevertheless, despite changes in the specific products employed, the fundamentals of our methods should remain viable for a long time. It is likely that more and more low cost, high-speed video cameras will become available. The same is true for laser light sources. For only a slightly greater cost, for example, much stronger laser pointers than the one we used, as well as other laser light sources, are offered on the market. There are multiple software products, both commercial and open-source that are available to accomplish the tasks we outline and it is also likely that these will only increase in number. At the same time, research-grade equipment, particular high-speed video cameras, is becoming less costly. Although specific components might change, we believe that the basic, low cost DPIV system we describe here will remain a useful alternative for years to come.

ACKNOWLEDGMENTS

We are very grateful to Lauren Jones and Sara Horwitz for their help. Karolina Fucikova generously provided us with algae and her expertise in growing it. We benefitted a great deal from discussions with Diego Sustaita and other members of the Beermorph group. The comments of two anonymous reviewers were exceptionally helpful in improving the manuscript. Work was supported financially by the Wetzel Fund of the Department of Ecology and Evolutionary Biology (to W.R.) and the University of Connecticut Research Foundation (to K.S.).

LITERATURE CITED

Adrian RJ. 2005. Twenty years of particle image velocimetry. Exp Fluids 39:159–169.

Altshuler DL, Princevac M, Pan H, Lozano J. 2009. Wake patterns of the wings and tail of hovering hummingbirds. Exp Fluids 46:835–846.

Arnold S. 1983. Morphology, performance and fitness. Am Zool 23:347–361.

Bergmann PJ, Irschick DJ. 2010. Alternate pathways of body shape evolution translate into common patterns of locomotor evolution in two clades of lizards. Evolution 64:1569–1582.

Bold HC. 1949. The morphology of *Chlamydomonas chlamydogama*, sp. nov. Bull Torrey Bot Club 76:101–108.

Crimaldi JP, Koehl MAR, Koseff JR. 2002. Effects of the resolution and kinematics of olfactory appendages on the interception of

chemical signals in a turbulent odor plume. Environ Fluid Mech 2:35–63.

Day SW, Higham TE, Cheer AY, Wainwright PC. 2005. Spatial and temporal patterns of water flow generated by suction-feeding bluegill sunfish *Lepomis macrochirus* resolved by particle image velocimetry. J Exp Biol 208:2661–2671.

Day SW, Higham TE, Wainwright PC. 2007. Time resolved measurements of the flow generated by suction feeding fish. Exp Fluids 43:713–724.

Deng Z, Richmond MC, Guensch GR, Mueller RP. 2004. Study of fish response using particle image velocimetry and high-speed, high-resolution imaging. US Department of Energy, Pacific Northwest National Laboratory (PNNL 14819). Springfield, VA: National Technical Information Service. p 1–45.

Filoramo N, Schwenk K. 2009. The mechanism of chemical delivery to the vomeronasal organs in squamate reptiles: a comparative morphological approach. J Exp Zool (Ecol Gen Physiol) 311A:20–34.

Fincham AM, Spedding JR 1997. Low cost, high resolution DPIV for measurement of turbulent fluid flow. Exp Fluids 23:449–462.

Garcia D. 2010. Robust smoothing of gridded data in one and higher dimensions with missing values. Comput Stat Data Anal 54:1167–1178.

Goldman JA, Patek SN. 2002. Two sniffing strategies in palinurid lobsters. J Exp Biol 205:3891–3902.

Gove D. 1979. A comparative study of snake and lizard tongue-flicking, with an evolutionary hypothesis. Z Tierpsychol 51:58–76.

Halpern M. 1992. Nasal chemical senses in reptiles: structure and function. In: Gans C, Crews D, editors. Hormones, brain and behavior. Biology of the Reptilia, physiology E. Chicago: University of Chicago Press. p 423–523.

Huang H, Dabiri D, Gharid M. 1997. On errors of digital image velocimetry. Meas Sci Technol 8:1427–1440.

Hedenström A, Muijres FT, von Busse R, Johansson LC, Winter Y, Spedding GR. 2009. High-speed stereo DPIV measurement of wakes of two bat species. Exp Fluids 46:923–932.

Herrel A, Vincent SE, Alfaro ME, Wassenbergh S, Irschick DJ. 2008. Morphological convergence as a consequence of extreme functional demands: examples from the feeding system of natricine snakes. J Evol Biol 21:1438–1448.

Holzman R, Collar DC, Day SW, Bishop KL, Wainwright PC. 2008. Scaling of suction-induced flows in bluegill: morphological and kinematic predictors for the ontogeny of feeding performance. J Exp Biol 211:2658–2668.

Koehl MAR. 1996. When does morphology matter? Ann Rev Ecol Syst 27:501–542.

Koehl MAR. 2001. Fluid dynamics of animal appendages that capture molecules: arthropod olfactory antennae. In: Fauci LJ, Gueron S, editors. Computational modeling in biological fluid dynamics. New York: Springer. p 97–116.

Koehl MAR. 2003. Physical modeling in biomechanics. Philos Trans R Soc Lond B Biol Sci 358:1589–1596.

Koehl MAR, Koseff JR, Crimaldi JP, McCay MG, Cooper T, Wiley MB, Moore PA. 2001. Lobster sniffing: antennule design and hydrodynamic filtering of information in an odor plume. Science 294:1948–1951.

Lauder GV. 2011. Swimming hydrodynamics: ten questions and the technical approaches needed to resolve them. Exp Fluids 51:23–35.

Lauder GV, Madden PGA. 2008. Advances in comparative physiology from high-speed imaging of animal and fluid motion. Ann Rev Physiol 70:143–163.

Loudon C, Koehl MAR. 2000. Sniffing by a silkworm moth: wing fanning enhances air penetration through and pheromone interception by antennae. J Exp Biol 203:2977–2990.

Loudon C, Best BA, Koehl MAR. 1994. When does motion relative to neighboring surfaces alter the flow through arrays of hairs? J Exp Biol 193:233–254.

McKeon BJ, Comte-Bellot G, Foss JF, Westerweel J, Scarano F, Tropea C, Meyers JF, Lee JW, Cavone AA, Schodl R, Koochesfahani MM, Andreopoulos Y, Dahm WJA, Mullin JA, Wallace JM, Vukoslavcevic PV, Morris SC, Pardyjak ER, Cuerva A. 2007. Velocity, vorticity, and mach number. In: Tropea C, Yarin AL, Foss JF, editors. Springer handbook of experimental fluid mechanics. Berlin: Springer. p 215–472.

Mead KS, Wiley MB, Koehl MAR, Koseff JR. 2003. Fine-scale patterns of odor encounter by the antennules of mantis shrimp tacking turbulent plumes in wave-affected and unidirectional flow. J Exp Biol 206:181–193.

Moore P, Crimaldi J. 2004. Odor landscapes and animal behavior: tracking odor plumes in different physical worlds. J Mar Sci 49:55–64.

Mountcastle AM, Daniel TL. 2009. Aerodynamic and functional consequences of wing compliance. Exp Fluids 46:873–882.

Nauwelaerts S, Wilga CD, Lauder GV, Sanford CP. 2008. Fluid dynamics of feeding behaviour in white-spotted bamboo sharks. J Exp Biol 211:3095–3102.

Oliver RL, Kinnear AJ, Ganf GG. 1981. Measurements of cell density of three freshwater phytoplanksters by density gradient centrifugation. Limnol Oceanogr 26:185–294.

Prasad AK. 2000. Particle image velocimetry. Curr Sci 79:51–60.

Prasad AK, Adrian RJ, Landreth CC, Offutt PW. 1992. Effect of resolution on the speed and accuracy of particle image velocimetry interrogation. Exp Fluids 13:105–116.

Raffel M, Willert C, Kompenhans J. 2000. Particle image velocimetry: a practical guide. Berlin: Springer.

Ram JL, Fei X, Danaher SM, Lu S, Breithaupt T, Hardege JD. 2008. Finding females: pheromone-guided reproductive tracking behavior by male *Nereis succinea* in the marine environment. J Exp Biol 211:757–765.

Schoenfeld TA, Cleland TA. 2005. The anatomical logic of smell. Trends Neurosci 28:620–627.

Schwenk K. 1995. Of tongues and noses: chemoreception in lizards and snakes. Trends Ecol Evol 10:7–12.

Schwenk K. 1996. Why snakes flick their tongues. Am Zool 36:84A (abstract).

Spedding GR, Hedenström A. 2009. PIV-based investigations of animal flight. Exp Fluids 46:749–763.

Spedding GR, Hedenström A, Rosén M. 2003. Quantitative studies of the wakes of freely flying birds in a low-turbulence wind tunnel. Exp Fluids 34:291–303.

Tobalske B. 2007. Biomechanics of bird flight. J Exp Biol 210:3135–3146.

Tobalske BW, Hearn JWD, Warrick DR. 2009. Aerodynamics of intermittent bounds in flying birds. Exp Fluids 46:963–973.

Vogel S. 1994. Life in moving fluids. The physical biology of flow, 2nd edition. Princeton: Princeton University Press.

Vogel S. 2003. Comparative biomechanics. Life's physical world. Princeton: Princeton University Press.

Wang S, Pu Y, Jia F, Gutkowski A. 2006. Effect of turbulence on flame propagation in cornstarch dust-air mixtures. J Therm Sci 15:186–192.

Yang J, Sliva A, Banerjee A, Dave RN, Pfeffer R. 2005. Dry particle coating for improving the flowability of cohesive powders. Powder Technol 158:21–33.